

Article

# Bridgman Growth of New Nonlinear Optical Crystal $(\text{La}_{1-x}\text{Sm}_x)_3\text{Ga}_{5.5}\text{Nb}_{0.5}\text{O}_{14}$ for Quasi-Parametric Chirped Pulse Amplification

Libin Yin <sup>1,2</sup>, Sheng Wang <sup>2,3</sup>, Kainan Xiong <sup>2</sup>, Xiaoniu Tu <sup>2,3</sup> , Jiayue Xu <sup>1,\*</sup>, Yanqing Zheng <sup>2,\*</sup> and Erwei Shi <sup>2</sup>

<sup>1</sup> School of Materials Science and Engineering, Shanghai Institute of Technology, Shanghai 201418, China; Libin\_Yin@163.com

<sup>2</sup> Shanghai Institute of Ceramics, Chinese Academy of Sciences, Shanghai 201899, China; wangsheng@mail.sic.ac.cn (S.W.); xiongakainan@mail.sic.ac.cn (K.X.); xiaoniu\_tu@mail.sic.ac.cn (X.T.); ewshi@mail.sic.ac.cn (E.S.)

<sup>3</sup> Suzhou Research Institute, Shanghai Institute of Ceramics, Chinese Academy of Sciences, 6 Liangfu Road, Taicang, Jiangsu 215400, China

\* Correspondence: xujiayue@sit.edu.cn (J.X.); zyq@mail.sic.ac.cn (Y.Z.); Tel.: +86-136-2195-7575 (J.X.); +86-133-0168-7112 (Y.Z.)

Received: 13 October 2019; Accepted: 7 November 2019; Published: 9 November 2019



**Abstract:** Samarium-doped  $\text{La}_3\text{Nb}_{0.5}\text{Ga}_{5.5}\text{O}_{14}$  (Sm:LGN) crystals were grown along a (100)-orientation by the Bridgman method for quasi-parametric chirped pulse amplification (QPCPA) applications. The structure of  $\text{La}_{1-x}\text{Sm}_x\text{mGN}$  ( $x = 0.1, 0.2$ ) crystals was the same as that of  $\text{La}_3\text{Nb}_{0.5}\text{Ga}_{5.5}\text{O}_{14}$  (LGN) crystals. The effective segregation coefficient of  $\text{Sm}^{3+}$  in the  $\text{La}_{0.9}\text{Sm}_{0.1}\text{GN}$  crystal was 0.140. The full width at half maximum (FWHM) of  $\text{La}_{1-x}\text{Sm}_x\text{mGN}$  ( $x = 0.1, 0.2$ ) crystals was lower than  $50''$ , which indicated the high quality of the crystals. The density of the  $\text{La}_{0.9}\text{Sm}_{0.1}\text{GN}$  crystal was  $5.968 \text{ g/cm}^3$  and that of the  $\text{La}_{0.8}\text{Sm}_{0.2}\text{GN}$  crystal was  $5.988 \text{ g/cm}^3$ . The transmittance of the crystals at 532nm and 800nm was all above 73%. The absorption spectra indicated that the crystals had strong absorption peaks at wavelengths of 1544 and 1595 nm. The thermal properties of  $\text{La}_{1-x}\text{Sm}_x\text{mGN}$  ( $x = 0.1, 0.2$ ) crystals were similar to those of the LGN crystals. The laser damage thresholds of  $\text{La}_{0.9}\text{Sm}_{0.1}\text{GN}$  and  $\text{La}_{0.8}\text{Sm}_{0.2}\text{GN}$  crystals were, respectively, 188.30 and  $54.84 \text{ TW/cm}^2$  (@800 nm, 35 fs).

**Keywords:** Bridgman growth; nonlinear optics crystal; Sm-doped;  $\text{La}_3\text{Ga}_{5.5}\text{Nb}_{0.5}\text{O}_{14}$

## 1. Introduction

Since the invention of laser technology, many scientists have focused their efforts on obtaining ultra-intense and ultra-short laser pulses. Chirped-pulse amplification (CPA), which won the Nobel Prize in physics in 2018, was first reported in 1985 [1]. The CPA scheme firstly involves the stretch of a femtosecond pulse, followed by amplification and, finally, compression to obtain a high peak power. Nowadays, the main crystal used in the CPA scheme is Ti:sapphire. The conversion efficiency of CPA can be up to 50% [2,3]. However, the gain in bandwidth is limited due to the presence of sharp energy levels. The gain bandwidth is only 75 nm at 800 nm when using the Ti:sapphire amplifier [4]. After the invention of the CPA scheme, optical parametric chirped-pulse amplification (OPCPA) was proposed by Dubietis et al. in 1992 [5]. The amplification process of OPCPA is completed by nonlinear parametric amplification in which the energy level is virtual and tunable. As such, the OPCPA scheme can obtain a wider gain in bandwidth. Furthermore, the thermal effect of OPCPA is weak. Nevertheless, the conversion efficiency of OPCPA is lower because of the backflow effect and strict phase matching condition. The crystals that can be used in OPCPA include BBO ( $\beta\text{-BaB}_2\text{O}_4$ ),

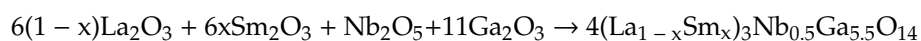
LBO ( $\text{LiB}_3\text{O}_5$ ), KDP ( $\text{KH}_2\text{PO}_4$ ), CLBO ( $\text{CsLiB}_6\text{O}_{10}$ ), YCOB ( $\text{YCa}_4\text{O}(\text{BO}_3)_3$ ), LGN ( $\text{La}_3\text{Ga}_{5.5}\text{Nb}_{0.5}\text{O}_{14}$ ) and so on [6,7]. In order to obtain a high conversion efficiency and broad bandwidth at the same time, Qian and Zheng et al. reported a new scheme termed quasi-parametric chirped pulse amplification (QPCPA) in 2015 [8]. The only (but important) difference between OPCPA and QPCPA is the nonlinear crystal which is used. The QPCPA uses a specific crystal to absorb the idler wave. The QPCPA can obtain a high conversion efficiency and wide gain in bandwidth at the same time. Furthermore, the QPCPA is insensitive to phase matching. Nowadays, only Sm:YCOB crystals are reported to be used in QPCPA [9]. The YCOB crystal has a wide range of applications in piezoelectric and nonlinear optics fields. Although the Sm:YCOB crystal has been verified in QPCPA, its transmittance and crystal size limit its wider application. The transmittance range of YCOB crystal is 0.5–2.5  $\mu\text{m}$  [10]. Two cleavage planes of YCOB crystal are, respectively,  $(\bar{2}01)$  and  $(101)$  [11], so it is difficult to obtain high-quality YCOB crystals with an aperture larger than 100 mm. The transmittance of the LGN crystal is 0.28–7.5  $\mu\text{m}$ , which is wider than that of the YCOB crystal; therefore, the LGN crystal has a wider range of application. Furthermore, the LGN crystal has no cleavage plane compared with the YCOB crystal. Therefore, the LGN crystal can easily exist as large-sized single crystals. In 2014, Patricia Segonds et al. reported nonlinear properties of the  $\text{La}_3\text{Ga}_5\text{SiO}_{14}$  (LGT) crystal [12]. Furthermore, the Sm-doped LGT crystals were also studied by Kaczmarek et al in detail. The magnetic and spectroscopic properties of Sm:LGT were measured [13,14]. Later, further research was carried out on the LGN crystal by Yu et al., [15]. Furthermore, theoretical research was also reported on the LGN crystal in optical parametric chirped pulse amplification (OPCPA), which demonstrates that the LGN crystal is a promising nonlinear optical crystal material [16].

The  $\text{La}_3\text{Ga}_5\text{SiO}_{14}$  (LGS, langasite) crystal was firstly produced in 1983 by Kaminsky et al through the Czochralski method as a laser crystal [17]. Since the LGS crystal was reported, the isomorphic compounds of LGS,  $\text{La}_3\text{Ta}_{0.5}\text{Ga}_{5.5}\text{O}_{14}$  (LGT, langatate), and  $\text{La}_3\text{Nb}_{0.5}\text{Ga}_{5.5}\text{O}_{14}$  (LGN, langanate) have also been obtained. The electro-optic, piezoelectric, and dielectric properties of these crystals were also intensively studied [18]. These crystals are important single crystals because they do not undergo a phase transition when they reach the melting point [19]. Nowadays, most of the langasite-type crystals are grown by the Czochralski method, and only a few of these crystals are grown by the Bridgman method, such as  $\text{La}_3\text{GaSi}_5\text{O}_{14}$  (LGS),  $\text{Sr}_3\text{Ga}_2\text{Ge}_4\text{O}_{14}$  (SGG),  $\text{Ca}_3\text{TaGa}_3\text{Si}_2\text{O}_{14}$  (CTGS),  $\text{Ca}_3\text{NbGa}_3\text{Si}_2\text{O}_{14}$  (CNGS), and  $\text{Sr}_3\text{NbGa}_3\text{Si}_2\text{O}_{14}$  (SNGS) crystals [20–22]. To the best of our knowledge, the LGN crystal has not reported to be grown by the Bridgman method. The LGN crystal reported for OPCPA was grown by the Czochralski method. However, the cost of the Czochralski method is higher than that of the Bridgman method, therefore, it is not suitable for industrial production. Furthermore, the pump wave and signal wave are, respectively, 532 nm and 800 nm, and the idle wave is around 1588 nm, so we replace  $\text{La}^{3+}$  with the  $\text{Sm}^{3+}$  ion to absorb the idle wave.

In this paper,  $(\text{La}_{1-x}\text{Sm}_x)_3\text{Nb}_{0.5}\text{Ga}_{5.5}\text{O}_{14}$  ( $x = 0.1, 0.2$ ) crystals were grown by the Bridgman method. The structures, spectra, and thermal properties of  $(\text{La}_{1-x}\text{Sm}_x)_3\text{Nb}_{0.5}\text{Ga}_{5.5}\text{O}_{14}$  crystals were reported.

## 2. Materials and Methods

The starting materials used for crystal growth were prepared from a mixture of 4N pure  $\text{La}_2\text{O}_3$ ,  $\text{Sm}_2\text{O}_3$ ,  $\text{Ga}_2\text{O}_3$ , and  $\text{Nb}_2\text{O}_5$  powders weighed in stoichiometric proportions in the following reaction:



Because of the volatility of  $\text{Ga}_2\text{O}_3$ , 1 wt% of extra  $\text{Ga}_2\text{O}_3$  was added to compensate for the volatility during the crystal growth process. The raw materials were ground, mixed uniformly, and pressed into blocks, before being sintered at 1200 to 1400  $^\circ\text{C}$  for at least 20 h to prepare the polycrystalline materials for crystal growth. The crystals of  $\text{La}_{1-x}\text{Sm}_x\text{GN}$  were grown by the Bridgman method. The growth direction was along (100). The crystallographic LGT crystal bars with  $\Phi 10\text{ mm} \times 60\text{ mm}$  were used as seed crystals. The Pt crucible was 10 mm in diameter and 150 mm in length. The furnace

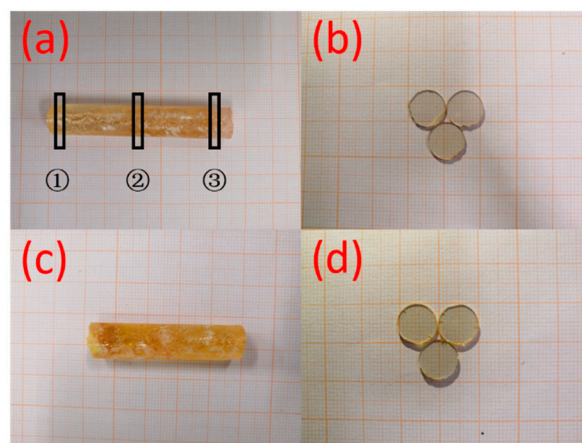
temperature was set to about 1600 °C, and the growth rate was less than 1 mm/h. When the crystal growth process was over, the temperature cooled down to room temperature at 40 °C/h.

X-ray diffraction (XRD, Rigaku, Tokyo, Japan) was used to identify the phase of the grown crystals. XRD data of the crystal sample were collected on a Rigaku D/max 2550 V diffractometer. High-resolution X-ray diffraction (HRXRD) (Bruker, Karlsruhe, Germany) was used to characterize the quality of crystals by D8-discover. The transmission and absorption spectra of the (100)-orientation wafer from 0.2 to 2.5 μm were measured by the Carry 5000 UV-Vis-NIR (Agilent, Palo Alto, CA, USA), and from 2.5 to 10 μm were measured by the Nicolet 6700 (Thermo, MA, USA) instrument at room temperature. The effective segregation coefficient of Sm<sup>3+</sup> in the crystal was determined by X-ray fluorescence analysis (PANalytical, Almelo, Netherlands). The thermal properties of crystals were also tested. The density of the crystals was measured by the Archimedes-method. The specific heat of these crystals was measured by DSC-MHTC96 (Setaram, Leon, France). NETZSCH LFA 457 (NETZSCH, Selb, Germany) was used to measure the thermal diffusion coefficient of La<sub>1-x</sub>Sm<sub>x</sub>GN crystals. The thermal conductivity was calculated by the density, specific heat, and thermal diffusion coefficient of crystals. The laser damage threshold was measured at 800 nm, with a pulse width of 35 fs.

### 3. Results and Discussion

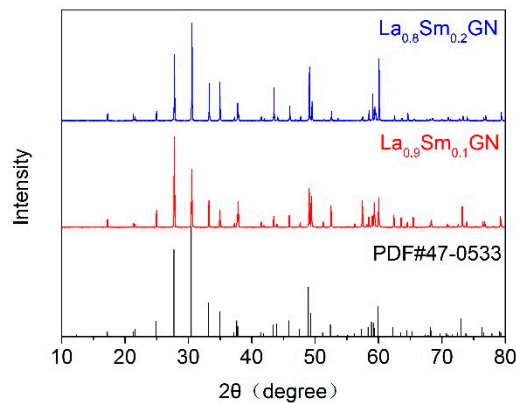
#### 3.1. Crystal Growth and Characterization

The crystals which were grown by the Bridgman method with different Sm<sup>3+</sup> concentrations, which are shown in Figure 1. There were a few expelled impurities observable on the top of the crystals. The diameters of the crystals were 10 mm with a length of 50 to 65 mm. Because of the stripping of the Pt crucible from the crystals, the surface of the crystals was opaque. As shown in Figure 1b,d, the crystals were transparent after cutting and polishing.



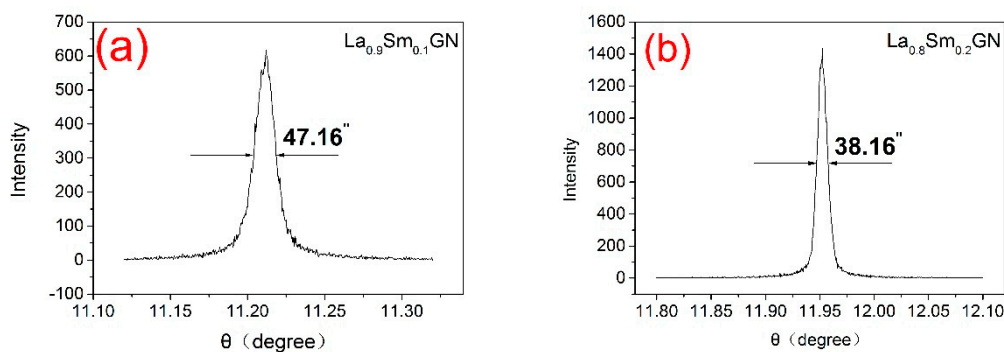
**Figure 1.** Samarium-doped La<sub>3</sub>Nb<sub>0.5</sub>Ga<sub>5.5</sub>O<sub>14</sub> (Sm:LGN) crystals grown by the Bridgman method. (a) and (b) La<sub>0.9</sub>Sm<sub>0.1</sub>GN, (c) and (d) La<sub>0.8</sub>Sm<sub>0.2</sub>GN.

Figure 2 shows the XRD patterns of the as-grown La<sub>1-x</sub>Sm<sub>x</sub>GN ( $x = 0.1, 0.2$ ) crystals compared with the pure LGN crystals. It can be seen that La<sub>1-x</sub>Sm<sub>x</sub>GN crystals have the same structure as pure LGN crystals, which indicates that La<sub>1-x</sub>Sm<sub>x</sub>GN crystals still belong to the P321 space group and 32 trigonal point group.



**Figure 2.** The X-ray diffraction (XRD) patterns of the Sm:LGN crystals.

In order to evaluate the crystal quality, the rocking curve of polished (100)-orientation wafers were scanned on HRXRD. The rocking curves of the wafers are shown in Figure 3. The full width at half maximum (FWHM) values of the rocking curves of the polished wafers, with different  $\text{Sm}^{3+}$  concentrations were all lower than  $50''$ . The FWHM values of  $\text{La}_{0.9}\text{Sm}_{0.1}\text{GN}$  and  $\text{La}_{0.8}\text{Sm}_{0.2}\text{GN}$  crystals were, respectively,  $47.16''$  and  $38.16''$ . The results show that the as-grown crystals were of good quality.



**Figure 3.** High resolution X-ray diffraction (HRXRD) results of (100)-orientation wafers of Sm:LGN crystals. (a)  $\text{La}_{0.9}\text{Sm}_{0.1}\text{GN}$  and (b)  $\text{La}_{0.8}\text{Sm}_{0.2}\text{GN}$ .

Because the seed crystals were LGT crystals, so it was necessary to measure the compositions of the crystals. The bottom, middle, and top of the crystal, shown, respectively, as ①, ② and ③ in Figure 1a, were selected to perform the XRF. The results are shown in Tables 1 and 2. The effective segregation coefficient of Sm:LGN crystals can be calculated by the following equation:

$$K_{\text{eff}} = C_{\text{bottom}}/C_0,$$

where  $C_{\text{bottom}}$  is the concentration of  $\text{Sm}^{3+}$  in the starting position of crystal growth, and the  $C_0$  is the initial concentration in the melt that is used to grow the crystal. The results measured by XRF of the 10 at% Sm:LGN crystal are listed in Table 1. The effective segregation coefficient is  $K_{\text{eff}} = 0.140$ , which indicates serious segregation of the Sm:LGN crystals. The density of crystals was measured by the Archimedes-method at room temperature. The density of  $\text{La}_{0.9}\text{Sm}_{0.1}\text{GN}$  was  $5.968 \text{ g/cm}^3$  and that of  $\text{La}_{0.8}\text{Sm}_{0.2}\text{GN}$  was  $5.988 \text{ g/cm}^3$ .

**Table 1.** The XRF results of Sm in 10 at% Sm:LGN crystal.

Element	Bottom	Middle	Top	Solution (Theoretical)
Sm/wt%	0.83	2.38	3.47	4.20
Sm/at% (calculated)	1.40	3.84	5.65	10.00

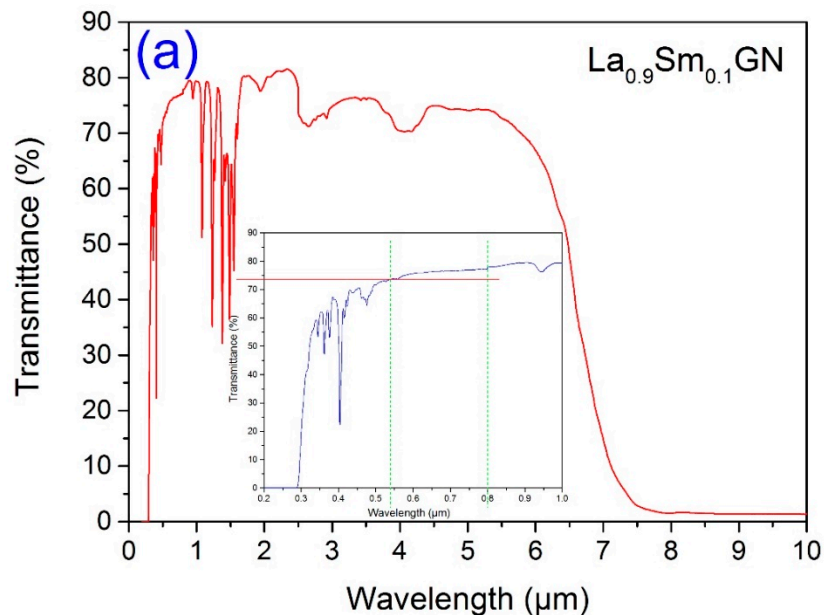
**Table 2.** The XRF results of the 10 at% Sm:LGN crystal.

Element	Bottom (wt%)	Middle (wt%)	Top (wt%)
La	40.55	40.12	39.49
Ga	31.09	33.29	32.87
Nb	1.26	5.29	5.32
Ta	6.42	0.47	0.46
Sm	0.83	2.38	3.47

From Table 2, we can see that the content of Ta was higher at the bottom than that at the middle and top of the crystal. The reason for this phenomenon is that the seed crystal we used was LGT crystal. The LGT crystal melted during inoculation and brought the Ta element into the crystal, which was grown by the Bridgman method. Since there was a lower concentration of Ta element, except for in the bottom of the crystal, we considered the crystal to be approximately pure Sm:LGN crystal.

### 3.2. Spectral Properties

One-millimeter-thick (100)-orientation slabs of crystals with a diameter of 10 mm, which were polished and uncoated, were used to test the transmission and absorption spectra. The results of the transmission spectra are shown in Figure 4. The results show that the doping of Sm ions has no effect on the UV and infrared cut-off edges. The transmittance of the crystals at 532 nm and 800 nm was as high as 73%, which is advantageous for device application.

**Figure 4.** Cont.

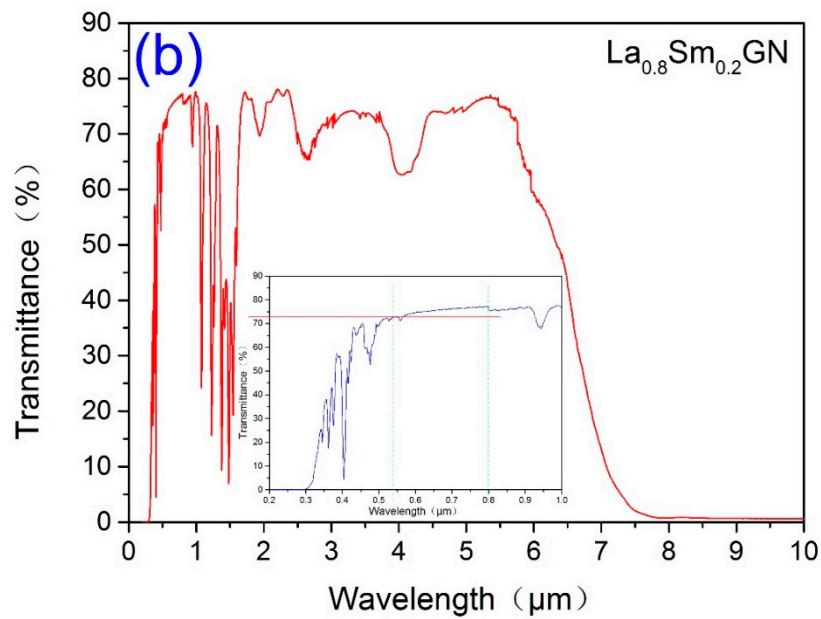


**Figure 4.** The transmission spectra of Sm:LGN crystals: (a)  $\text{La}_{0.9}\text{Sm}_{0.1}\text{GN}$  and (b)  $\text{La}_{0.8}\text{Sm}_{0.2}\text{GN}$ .

Figure 5 presents the absorption spectra of as-grown single crystals measured from 500 to 2500 nm. We can see that the crystals have two evident absorption peaks near a wavelength of 1588 nm. The two absorption peaks at 1544 and 1595 nm, respectively, result from  ${}^6\text{H}_{5/2} \rightarrow {}^6\text{F}_{1/2}$  and  ${}^6\text{H}_{5/2} \rightarrow {}^6\text{H}_{15/2}$  transitions. It can be seen that the intensity of the absorption peak becomes stronger with the increasing concentration of  $\text{Sm}^{3+}$ . Furthermore, there are no evident peaks near the pump wavelength of 532 nm and the signal wavelength of 800 nm, which indicate that the crystals are suitable for the QPCPA scheme.

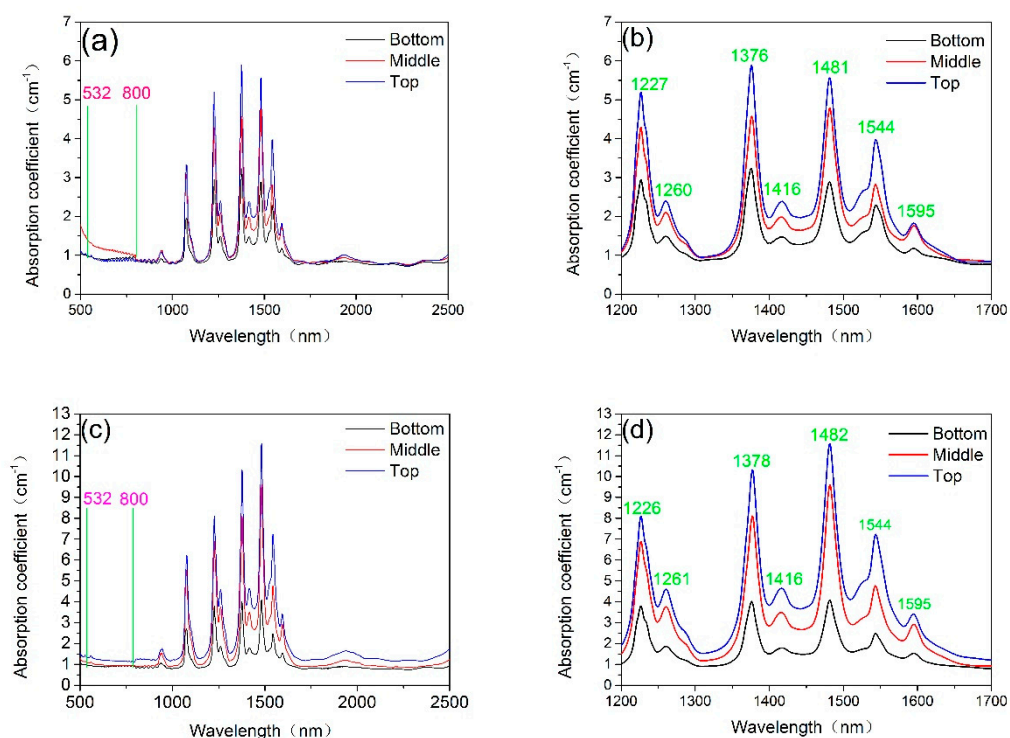


**Figure 5.** The absorption spectra of Sm:LGN crystals: (a) and (b)  $\text{La}_{0.9}\text{Sm}_{0.1}\text{GN}$ ; (c) and (d)  $\text{La}_{0.8}\text{Sm}_{0.2}\text{GN}$ .

### 3.3. Thermal Properties

The size of the samples measured for their specific heat was  $4 \times 4 \times 0.5 \text{ mm}^3$ , and the (100)-orientation samples were polished and uncoated. The thermal diffusion coefficient was measured with  $\Phi 10 \times 1 \text{ mm}$  wafers of (100)-orientation. Figure 6a shows the specific heat results of as-grown crystals, which were measured from room temperature to 573.15 K. We can see that the specific heat rose as the temperature increased. The  $\text{La}_{0.9}\text{Sm}_{0.1}\text{GN}$  crystal changed from  $0.4 \text{ J/g}^{-1}\text{K}^{-1}$  to  $0.514 \text{ J/g}^{-1}\text{K}^{-1}$  and that of  $\text{La}_{0.8}\text{Sm}_{0.2}\text{GN}$  rose from  $0.394 \text{ J/g}^{-1}\text{K}^{-1}$  to  $0.508 \text{ J/g}^{-1}\text{K}^{-1}$ . Both of the  $\text{La}_{1-x}\text{Sm}_x\text{GN}$  crystals had higher values than the LGN crystal. The results of specific heat indicate that the new crystals are suitable for used in high-power lasers. The thermal diffusion coefficient of crystals is shown in Figure 6b. It can be seen that the thermal diffusion coefficient decreased when the temperature increased. However, both of the  $\text{La}_{1-x}\text{Sm}_x\text{GN}$  crystals containing the Sm element had lower values than the LGN crystal.

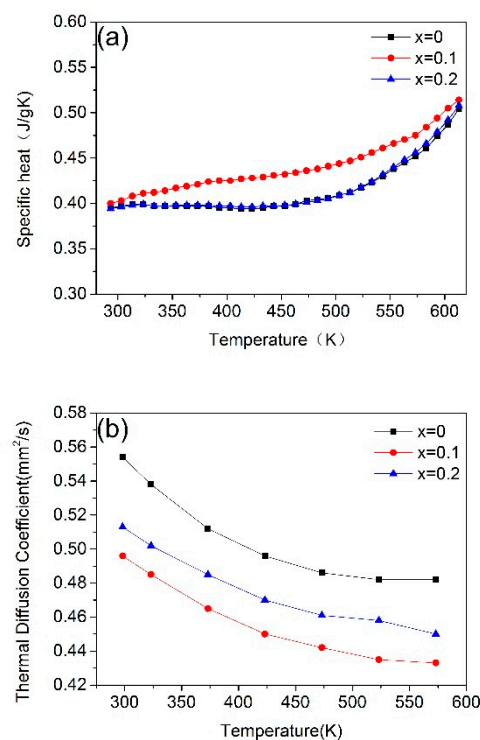


**Figure 6.** The specific heat (a) and thermal diffusion coefficient (b) of Sm:LGN crystals.

The results of the thermal conductivity of crystals which are also of great importance, can be calculated by the following equation:

$$K = \lambda \rho C_p,$$

where  $K$  is the thermal conductivity,  $\lambda$ ,  $\rho$ , and  $C_p$ , respectively, denote the thermal diffusion coefficient, the density, and the specific heat of the crystal. The calculated results are plotted in Figure 7. The thermal conductivity of as-grown crystals decreased when the temperature reached 500 K and then rose again. The minimum value of specific heat of the crystals was obtained between 425 and 475 K. Compared with the LGN crystal, the maximum reduction in the thermal conductivity was 4.18%. The laser damage threshold was measured at 800 nm with a pulse width of 35 fs. The results of  $\text{La}_{0.9}\text{Sm}_{0.1}\text{GN}$  and  $\text{La}_{0.8}\text{Sm}_{0.2}\text{GN}$  crystals were, respectively,  $188.30 \text{ TW/cm}^2$  and  $54.84 \text{ TW/cm}^2$  lower than LGN crystals by a factor of two and a factor of six, respectively.

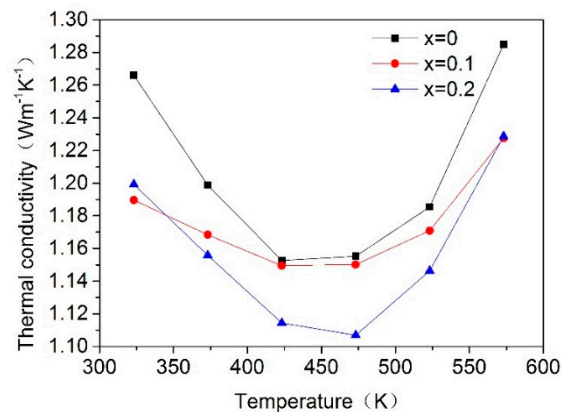


Figure 7. The thermal conductivity of Sm:LGN crystals.

#### 4. Conclusions

High quality  $\text{La}_{1-x}\text{Sm}_x\text{GN}$  ( $x = 0.1, 0.2$ ) single crystals were obtained by the Bridgman method and grown along the (100)-orientation. The results of XRD show that the crystals had the same structure as the LGN crystal. The HRXRD results show that the quality of the crystals was good. The segregation coefficient of the  $\text{La}_{0.9}\text{Sm}_{0.1}\text{GN}$  crystal was 0.140. The densities of the  $\text{La}_{0.9}\text{Sm}_{0.1}\text{GN}$  and  $\text{La}_{0.8}\text{Sm}_{0.2}\text{GN}$  crystals were, respectively,  $5.968 \text{ g/cm}^3$  and  $5.988 \text{ g/cm}^3$ . The  $\text{La}_{1-x}\text{Sm}_x\text{GN}$  ( $x = 0.1, 0.2$ ) crystals had no absorption peaks at 532 nm and 800 nm. Furthermore, the crystals demonstrated strong absorption at the wavelengths of 1544 and 1595 nm, including that the crystals can be used in QPCPA applications. The results of specific heat, thermal diffusion coefficient, and thermal conductivity show that  $\text{La}_{1-x}\text{Sm}_x\text{GN}$  ( $x = 0.1, 0.2$ ) crystals have similar thermal properties to the LGN crystal. The laser damage threshold of  $\text{La}_{0.9}\text{Sm}_{0.1}\text{GN}$  and  $\text{La}_{0.8}\text{Sm}_{0.2}\text{GN}$  crystals were found to be  $188.30 \text{ TW/cm}^2$  and  $54.84 \text{ TW/cm}^2$  (@800 nm, 35 fs), respectively, which indicated that the  $\text{La}_{1-x}\text{Sm}_x\text{GN}$  crystals can be used in higher-power laser systems.

**Author Contributions:** Conceptualization, L.Y. and Y.Z.; funding acquisition, Y.Z., E.S. and X.T.; investigation, S.W., K.X. and L.Y.; methodology, L.Y., J.X., Y.Z. and S.W.; project administration, Y.Z. and E.S.; resources, J.X., Y.Z., S.W. and E.S.; writing (original draft), L.Y.; writing (review and editing), L.Y., Y.Z. and J.X.

**Funding:** This work was supported by the National Key Research and Development Plan (Grant No. 2016YFB0402701), the National Nature Science Foundation of China (Grant no. 51832009) and the Key Research and Development Program of Jiangsu Province (Grant NO. BE2018008-5).

**Conflicts of Interest:** The authors declare no conflicts of interest.

#### References

1. Strickland, D.; Mourou, G. Compression of amplified chirped optical pulses. *Opt. Commun.* **1985**, *55*, 447–449. [[CrossRef](#)]
2. Chu, Y.; Gan, Z.; Liang, X.; Yu, L.; Lu, X.; Wang, C.; Leng, Y. High-energy large-aperture Ti:sapphire amplifier for 5 PW laser pulses. *Opt. Lett.* **2015**, *40*, 5011. [[CrossRef](#)] [[PubMed](#)]
3. Sung, J.H.; Lee, H.W.; Yoo, J.Y.; Yoon, J.Y.; Lee, C.W.; Yang, J.M.; Son, J.Y.; Jang, J.H.; Lee, K.S.; Nam, C.H. 42 PW, 20 fs Ti:sapphire laser at 01 Hz. *Opt. Lett.* **2017**, *42*, 2058. [[CrossRef](#)] [[PubMed](#)]
4. Vaupel, A.; Bodnar, N.; Webb, B.; Shah, L.; Richardson, M.C. Concepts, performance review, and prospects of table-top, few-cycle optical parametric chirped-pulse amplification. *Opt. Eng.* **2013**, *53*, 051507. [[CrossRef](#)]
5. Dubietis, A.; Jonušauskas, G.; Piskarskas, A. Powerful femtosecond pulse generation by chirped and stretched pulse parametric amplification in BBO crystal. *Opt. Commun.* **1992**, *88*, 437–440. [[CrossRef](#)]
6. Mori, Y.; Nakajima, S.; Taguchi, A.; Miyamoto, A.; Inagaki, M.; Sasaki, T.; Nakai, S. New nonlinear optical crystal  $\text{CsLiB}_6\text{O}_{10}$  for laser fusion. *Aip Conf. Proc.* **1996**, *396*, 998–1003. [[CrossRef](#)]
7. Liao, Z.M.; Jovanovic, I.; Ebberts, C.A.; Fei, Y.; Chai, B. Energy and average power scalable optical parametric chirped-pulse amplification in yttrium calcium oxyborate. *Opt. Lett.* **2006**, *31*, 1277–1279. [[CrossRef](#)] [[PubMed](#)]

8. Ma, J.; Wang, J.; Yuan, P.; Xie, G.; Xiong, K.; Tu, Y.; Qian, L. Quasi-parametric amplification of chirped pulses based on a  $\text{Sm}^{3+}$ -doped yttrium calcium oxyborate crystal. *Optica* **2015**, *2*, 1006. [[CrossRef](#)]
9. Ma, J.; Wang, J.; Zhou, B.; Yuan, P.; Xie, G.; Xiong, K.; Qian, L. Broadband, efficient, and robust quasi-parametric chirped-pulse amplification. *Opt. Express* **2017**, *25*, 25149. [[CrossRef](#)] [[PubMed](#)]
10. Fei, Y.; Chai, B.H.; Ebberts, C.A.; Liao, Z.M.; Schaffers, K.I.; Thelin, P. Large-aperture YCOB crystal growth for frequency conversion in the high average power laser system. *J. Cryst. Growth* **2006**, *290*, 301–306. [[CrossRef](#)]
11. Tu, X.; Zheng, Y.; Xiong, K.; Shi, Y.; Shi, E. Crystal growth and characterization of 4in.  $\text{YCa}_4\text{O}(\text{BO}_3)_3$  crystal. *J. Cryst. Growth* **2014**, *401*, 160–163. [[CrossRef](#)]
12. Boursier, E.; Segonds, P.; Boulanger, B.; Félix, C.; Debray, J.; Jegouso, D.; Shoji, I. Phase-matching directions, refined Sellmeier equations, and second-order nonlinear coefficient of the infrared Langatate crystal  $\text{La}_3\text{Ga}_{5.5}\text{Ta}_{0.5}\text{O}_{14}$ . *Opt. Lett.* **2014**, *39*, 4033–4036. [[CrossRef](#)] [[PubMed](#)]
13. Kaczmarek, S.M.; Leniec, G.; Berkowski, M.; Kazan, S.; Açıkgöz, M. Magnetic properties of  $\text{La}_3\text{Ga}_{5.5}\text{Ta}_{0.5}\text{O}_{14}$  single crystals doped with  $\text{Sm}^{3+}$ . *J. Alloys Compd.* **2016**, *687*, 696–700. [[CrossRef](#)]
14. Komar, J.; Lisiecki, R.; Ryba-Romanowski, W.; Berkowski, M. Spectroscopic characterization of  $\text{Sm}^{3+}$  in  $\text{La}_3\text{Ga}_{5.5}\text{Ta}_{0.5}\text{O}_{14}$  single crystals. *J. Alloys Compd.* **2014**, *610*, 50–54. [[CrossRef](#)]
15. Lu, D.; Xu, T.; Yu, H.; Fu, Q.; Zhang, H.; Segonds, P.; Wang, J. Acentric langanite  $\text{La}_3\text{Ga}_{5.5}\text{Nb}_{0.5}\text{O}_{14}$  crystal: A new nonlinear crystal for the generation of mid-infrared parametric light. *Opt. Express* **2016**, *24*, 17603. [[CrossRef](#)] [[PubMed](#)]
16. Ma, J.; Wang, J.; Hu, D.; Yuan, P.; Xie, G.; Zhu, H.; Qian, L. Theoretical investigations of broadband mid-infrared optical parametric amplification based on a  $\text{La}_3\text{Ga}_{5.5}\text{Nb}_{0.5}\text{O}_{14}$  crystal. *Opt. Express* **2016**, *24*, 23957–23968. [[CrossRef](#)] [[PubMed](#)]
17. Kaminskii, A.A.; Mill, B.V.; Khodzhabyan, G.G.; Konstantinova, A.F.; Okorochkov, A.I.; Silvestrova, I.M. Investigation of trigonal  $(\text{La}_{1-x}\text{Nd}_x)_3\text{Ga}_5\text{SiO}_{14}$  crystals. I. Growth and optical Properties. *Phys. Status Solidi A* **1983**, *80*, 387–398. [[CrossRef](#)]
18. Bohm, J.; Heimann, R.B.; Hengst, M.; Roewer, R.; Schindler, J. Czochralski growth and characterization of piezoelectric single crystals with langasite structure:  $\text{La}_3\text{Ga}_5\text{SiO}_{14}$  (LGS),  $\text{La}_3\text{Ga}_{5.5}\text{Nb}_{0.5}\text{O}_{14}$  (LGN), and  $\text{La}_3\text{Ga}_{5.5}\text{Ta}_{0.5}\text{O}_{14}$  (LGT): Part I. *J. Cryst. Growth* **1999**, *204*, 128–136. [[CrossRef](#)]
19. Wang, S.Q.; Uda, S. Phase relations around langasite ( $\text{La}_3\text{Ga}_5\text{SiO}_{14}$ ) in the system  $\text{La}_2\text{O}_3$ – $\text{Ga}_2\text{O}_3$ – $\text{SiO}_2$  in air. *J. Cryst. Growth* **2003**, *250*, 463–470. [[CrossRef](#)]
20. Uda, S.; Inaba, H.; Harada, J.; Hoshikawa, K. Growth of langasite via Bridgman technique along  $[0111]$   $[\bar{2}\bar{1}\bar{1}0]$  and  $[01\bar{1}1]$  for piezoelectric applications. *J. Cryst. Growth* **2004**, *271*, 229–237. [[CrossRef](#)]
21. Zhou, J.; Xu, J.; Hua, W.; Fan, S. Bridgman growth of new piezoelectric single crystal  $\text{Sr}_3\text{Ga}_2\text{Ge}_4\text{O}_{14}$ . *Mater. Sci. Eng. B* **2004**, *106*, 213–217. [[CrossRef](#)]
22. Wu, A. Bridgman growth of langasite-type piezoelectric crystals. *Cryst. Res. Technol.* **2007**, *42*, 862–866. [[CrossRef](#)]

